Raman-noise induced quantum limits for $\chi^{(3)}$ nondegenerate phase-sensitive amplification and quadrature squeezing

Paul L. Voss, Kahraman G. Köprülü, and Prem Kumar

Center for Photonic Communication and Computing,
ECE Department, Northwestern University,
2145 Sheridan Road, Evanston, IL 60208-3118

We present a quantum theory of nondegenerate phase-sensitive parametric amplification in a $\chi^{(3)}$ nonlinear medium. The non-zero response time of the Kerr ($\chi^{(3)}$) nonlinearity determines the quantum-limited noise figure of $\chi^{(3)}$ parametric amplification, as well as the limit on quadrature squeezing. This non-zero response time of the nonlinearity requires coupling of the parametric process to a molecular-vibration phonon bath, causing the addition of excess noise through spontaneous Raman scattering. We present analytical expressions for the quantum-limited noise figure of frequency non-degenerate and frequency degenerate $\chi^{(3)}$ parametric amplifiers operated as phase-sensitive amplifiers. We also present results for frequency non-degenerate quadrature squeezing. We show that our non-degenerate squeezing theory agrees with the degenerate squeezing theory of Boivin and Shapiro as degeneracy is approached. We have also included the effect of linear loss on the phase-sensitive process.

OCIS codes: 060.2320, 270.5290.

1. Introduction

Fiber-optical parametric amplifiers (FOPAs) are currently the subject of much research for use in wavelength conversion[1] and efficient broadband amplification.[2] They are also candidates for performing all-optical network functions.[3,4,5] Advances in pumping techniques have permitted improvements of the noise figure (NF) of FOPAs operated phase-insensitively[1,6] and the manufacture of high-nonlinearity and microstructure fibers has improved the gain slope[7,8] of FOPAs.

In order to explain our experimental noise figure result for a phase-insensitive amplifier (PIA),[9] we have recently published a quantum theory of $\chi^{(3)}$ parametric amplifiers that takes into account the non-instantaneous nonlinear response of the medium and the requisite addition of noise caused by this non-instantaneous nonlinear response.[10,11] This work also provides analytical expressions for the noise figure of $\chi^{(3)}$ phase-insensitive parametric amplifiers[10] and wavelength converters (WCs).[11] This theory shows excellent agreement with experiment.[9] In addition, we have recently experimentally investigated the noise figure spectrum for PIA and WC operation of a FOPA, and shown good agreement to an extended theory that includes distributed loss.[12]

Phase-sensitive amplifiers (PSA)[13,14] are also of interest because unlike PIAs, they can ideally provide amplification without degrading the signal-to-noise ratio (SNR) at the input.[15] Experiments with fully frequency degenerate fiber phase-sensitive amplifiers have demonstrated a noise figure of 2.0 dB at a gain of 16 dB,[16] a value lower than the standard phase-insensitive high-gain 3-dB quantum limit. A noise figure below the standard PIA limit has also been reached in a low-gain phase-sensitive amplifier.[17] However, these fully frequency degenerate PSA experiments were impaired by guided-acoustic-wave Brillouin scattering (GAWBS)[18] requiring pulsed operation[19] or sophisticated techniques for partially suppressing GAWBS.[17] In order to avoid the GAWBS noise one may obtain phase-sensitive amplification with an improved experimental noise figure by use of a frequency nondegenerate PSA. In addition, the nondegenerate PSA, unlike its degenerate counterpart, can be used with multiple channels of data. A nondegenerate PSA is realized by placing the signal in two distinct frequency bands symmetrically around the pump frequency with a separation of several GHz, so that GAWBS noise scattered from the pump is not in the frequency bands of the signal. Such frequency nondegenerate regime has been demonstrated experimentally.[20] So an analysis of this case is practically useful. Accordingly, we here describe in suitable detail a quantum theory of FOPAs that takes into account the non-zero response time of the $\chi^{(3)}$ nonlinearity along with the effect of distributed linear loss. We present analytical expressions for the quantum-limited noise figure of CW $\chi^{(3)}$ PSAs in the frequency nondegenerate case. We also report the limiting value of the NF when degeneracy is approached.

A frequency nondegenerate parametric amplifier can also operate as a phase-sensitive deamplifier (PSD) of two-frequency input signals. When a PSD is operated with no input signal, such a parametric amplifier is said to produce "quadrature-squeezed vacuum" (parametric fluorescence of the PSD) whose two-frequency homodyne detection exhibits photocurrent variance less than that of the vacuum for suitable choice of homodyne phases.[21] Quadrature squeezing has been proposed for applications in quantum communications[22,23,24] and improved measurement sensitivity.[25] In the case of FOPAs, previous work by Shapiro and

Boivin[26] used the dispersionless theory of self-phase modulation (SPM) developed by Boivin and Kartner [27,28] that included the non-instantaneous response of the $\chi^{(3)}$ nonlinearity to obtain a limit on quadrature squeezing in the fully four-degenerate-wave case. In this paper, we present results for frequency nondegenerate CW quadrature squeezing for a noninstantaneous nonlinearity in the presence of dispersion. We show that optimal squeezing occurs for slightly different input conditions than those for optimal classical deamplification. In addition, we show that, unlike the dispersionless case, the degree of squeezing reaches a constant value in the long-interaction-length limit when the linear phase-mismatch is nonzero and a non-instantaneous nonlinear response is present. Our nondegenerate squeezing theory agrees with the previous degenerate squeezing results of Boivin and Shapiro[26] when degeneracy is approached.

This paper is organized as follows: In Section 2, we discuss the non-instantaneous $\chi^{(3)}$ nonlinear response. In Section 3 we discuss the solution of the equations describing evolution of the mean values of the pump, Stokes, and anti-Stokes fields. In Section 4, we present a quantum mechanically consistent theory of the FOPAs. In Sections 5 and 6, we apply this theory to obtain the noise figure of phase-sensitive amplification and to obtain the degree of nondegenerate quadrature squeezing, respectively. We reemphasize the main results and conclude in Section 7.

2. $\chi^{(3)}$ nonlinear response

We have discussed the $\chi^{(3)}$ nonlinear response at length;[11] only a summary is presented here. The nonlinear refractive index of the Kerr interaction can be written as

$$n_2 = \frac{3\chi^{(3)}}{4\epsilon_0 n_0^2 c}, \tag{1}$$

where n_0 is the linear refractive index of the nonlinear material, ϵ_0 is the permittivity of free space, and c is the speed of light in free space. For clarity, we state that

$$\chi^{(3)} \equiv \chi^{(3)}_{1111} \left[\frac{\mathrm{m}^2}{\mathrm{V}^2}\right]. \tag{2}$$

The $\chi^{(3)}(t)$ nonlinear response is composed of a time-domain delta-function-like electronic response ($\ll 1\,\mathrm{fs}$) that is constant in the frequency domain over the bandwidths of interest and a time-delayed Raman response ($\approx 50\,\mathrm{fs}$) that varies over frequencies of interest and is caused by back action of nonlinear nuclear vibrations on electronic vibrations. Recent experimental and theoretical results demonstrate that the nonlinear response function $\chi^{(3)}(t)$ can be treated as if it were real in the time domain,[29,30] yielding a real part that is symmetric in the frequency domain with respect to pump detuning and an imaginary part in the frequency domain that is anti-symmetric.

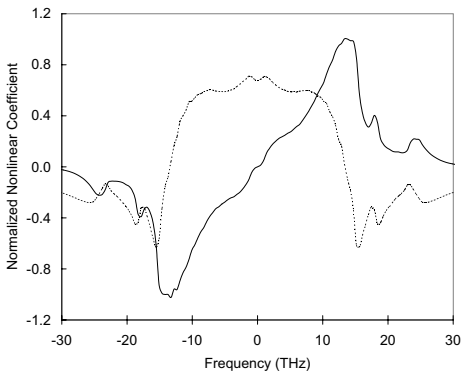

Fig. 1. Raman contribution $\mathrm{Im}\{\gamma_{\mathrm{Raman}\|}(\Omega)\}$ (solid curve) and $\mathrm{Re}\{\gamma_{\mathrm{Raman}\|}(\Omega)\}$ (dotted curve) normalized to the peak of $\mathrm{Im}\{\gamma_{\mathrm{Raman}\|}\}$. Calculated from Dougherty *et al.*[31]

Although a nonlinear response is also present in the polarization orthogonal to that of the pump, this cross-polarized nonlinear interaction is ignored because we assume that the pump, Stokes, and anti-Stokes fields of interest stay copolarized as their polarization states evolve during propagation through the FOPA. Parametric fluorescence and Raman spontaneous emission are present in small amounts in the polarization perpendicular to the pump, but do not affect the NF of the amplifier.

We can write $N_2(\Omega)$ in the frequency domain as a sum of electronic and molecular contributions:

$$N_2(\Omega) = n_{2\mathrm{e}} + n_{2\mathrm{r}} F(\Omega). \tag{3}$$

We next explain the relation between the published spectra of the Raman-gain coefficient and the nonlinear coefficients used in this paper. Typical measurements of the counterpropagating pump-and-signal Raman-gain spectrum yield the polarization averaged power-gain coefficient $g_{\mathrm{r}}(-\Omega) = [g_{\|}(-\Omega) + g_{\perp}(-\Omega)]/2$. At the Raman-gain peak, $g_{\perp} \simeq 0$, as can be seen from Fig. 1 of Dougherty *et al.*[31] We define a nonlinearity coefficient

$$\gamma_{\Omega} = \frac{2\pi N_2(\Omega)}{\lambda A_{\mathrm{eff}}}, \tag{4}$$

where λ is the pump wavelength and A_{eff} is the fiber effective area. Thus our γ_0 is equivalent to the nonlinear coupling coefficient γ used in Agrawal.[32] It is the scaling of A_{eff} with wavelength that mainly causes γ_{Ω} to be no longer anti-symmetric with $\gamma_{-\Omega}$ at detunings greater than several THz. In what follows, our analytical treatment of the mean fields allows for the more general case of asymmetry in the Raman-gain spectrum. However, other results including graphs assume an anti-symmetric Raman spectrum as this has a minor effect on the quantum noise at large detunings.

The above approximation is valid for our comparison to a typical experimental setup, wherein the pump-signal detuning is less than 1.5 THz. For co-propagating, co-polarized, optical waves $\mathrm{Im}\{\gamma_{-\Omega}\} = g_{\parallel}(-\Omega)/2$. We estimate the spectrum of $g_{\parallel}$, normalized to its maximum value, from Dougherty *et al.*[31] for both dispersion-shifted fiber (DSF) and standard single-mode fiber (SMF). From this normalized Raman-gain spectrum we obtain via the Kramers-Kronig transform the normalized real part of the spectrum of the Raman response, $\mathrm{Re}\{\gamma_{\mathrm{Raman}\parallel}(\Omega)\}$. In Fig. 1 the real (dotted curve) and imaginary parts (solid curve) of this spectrum are shown. We take the magnitude of the Raman-gain spectrum from Koch *et al.*[33] for both DSF and SMF. For $N_2(0)$, we use measurements from Boskovic *et al.*[34] The nonlinear coefficients are then calculated as follows:

$$\mathrm{Im}\{\gamma_{\Omega}\} = \frac{\mathrm{sgn}(\Omega) g_{\parallel\,\mathrm{normalized}}(\Omega) g_{\parallel\,\mathrm{peak}}}{2} \tag{5}$$

$$\mathrm{Re}\{\gamma_{\Omega}\} = \gamma_0 - \frac{\mathrm{Re}\{\gamma_{\parallel\mathrm{Raman}}(0)\} g_{\parallel\,\mathrm{peak}}}{2} + \frac{\mathrm{Re}\{\gamma_{\parallel\mathrm{Raman}}(\Omega)\} g_{\parallel\,\mathrm{peak}}}{2}, \tag{6}$$

where $\mathrm{Re}\{\gamma_{\parallel\mathrm{Raman}}(\Omega)\}$ is the Kramers-Kronig transform of $g_{\parallel\,\mathrm{normalized}}(\Omega)$.

3. Classical phase-sensitive amplification and deamplification

In this section we present solutions to the mean field equations (we denote mean fields with overbars) governing a parametric amplifier. The optical fields are assumed to propagate in a dispersive, polarization-preserving, single-transverse-mode fiber under the slowly-varying-envelope approximation. As the involved waves are quite similar in frequency, to good approximation all fields can be treated as if their transverse mode profiles are idententical. Even though the fibers used to construct FOPAs typically support two polarization modes and the polarization state of the waves is usually elliptical at a given point z in the FOPA, for typical fibers it is still appropriate to describe the system with a scalar theory if the detuning is relatively small.[12] This is because the input waves are copolarized at the beginning of the amplifier and the fields of interest remain essentially copolarized during propagation down the fiber.

Consider the field

$$\bar{A}(t) = \bar{A}_p + \bar{A}_s \exp(i\Omega t) + \bar{A}_a \exp(-i\Omega t) \tag{7}$$

for the total field propagating through a FOPA having a frequency and polarization degenerate pump. The lower frequency field we refer to as the Stokes field, $\bar{A}_s$; the higher frequency field referred to as the anti-Stokes field, $\bar{A}_a$. The classical equation of motion for the total field[35] with the addition of arbitrary frequency dependent loss is:

$$\frac{\partial \bar{A}(t)}{\partial z} = i\left[\int \mathrm{d}\tau\, \gamma(t-\tau)\bar{A}^*(\tau)\bar{A}(\tau)\right]\bar{A}(t) - \int \frac{\alpha(\Omega)}{2}\tilde{A}(\Omega)\exp(-i\Omega t)\,\mathrm{d}\Omega, \tag{8}$$

where $\alpha(\Omega)$ is the power attenuation coefficient at detuning Ω from the pump and $\widetilde{A}(\Omega)$ is the Fourier transform of the field. Because the involved waves (Stokes, anti-Stokes, and pump) are CW, the usual group-velocity dispersion term does not explicitly appear in Eq. (8). However, dispersion is included; its effect is simply to modify the wavevector of each CW component. Taking the Fourier transform of Eq. (8) and separating into frequency-shifted components that are capable of phase-matching, we obtain the following differential equations for the mean fields:[35]

$$\frac{\mathrm{d}\bar{A}_p}{\mathrm{d}z} = i\,\gamma_0\,|\bar{A}_p|^2\bar{A}_p - \frac{\alpha_p}{2}\bar{A}_p, \tag{9}$$

$$\frac{\mathrm{d}\bar{A}_a}{\mathrm{d}z} = i\,(\gamma_0+\gamma_\Omega)\,|\bar{A}_p|^2\bar{A}_a + i\gamma_\Omega\bar{A}_p^2\bar{A}_s^*\exp\left(-i\Delta k z\right) - \frac{\alpha_a}{2}\bar{A}_a, \tag{10}$$

$$\frac{\mathrm{d}\bar{A}_s}{\mathrm{d}z} = i\,(\gamma_0+\gamma_{-\Omega})\,|\bar{A}_p|^2\bar{A}_s + i\gamma_{-\Omega}\bar{A}_p^2\bar{A}_a^*\exp\left(-i\Delta k z\right) - \frac{\alpha_s}{2}\bar{A}_s. \tag{11}$$

Here $\Delta k = k_a + k_s - 2k_p$ is the phase mismatch. Expanding the wavevectors in a Taylor series around the pump frequency to second order, one obtains $\Delta k = \beta_2\Omega^2$ to second order, where β_2 is the group-velocity dispersion coefficient. The attenuation coefficients are α_j for $j = p, a, s$ at the pump, anti-Stokes, and Stokes wavelenths, respectively. The nonlinear coupling coefficients γ_0, γ_Ω, and $\gamma_{-\Omega}$ are as defined in the previous section. Eqs. (9–11) are valid when the pump remains essentially undepleted by the Stokes and anti-Stokes waves and is much stronger than the Stokes and anti-Stokes waves. The solution to Eqs. (9) and (11) can be expressed as

$$\bar{A}_a(z,L) = \mu_a(z,L)\bar{A}_a(z) + \nu_a(z,L)\bar{A}_s^*(z), \tag{12}$$

$$\bar{A}_s(z,L) = \mu_s(z,L)\bar{A}_s(z) + \nu_s(z,L)\bar{A}_a^*(z), \tag{13}$$

where we have explicitly written the solution as a function of both a starting point z for the parametric process and an end point L for the fiber. We do this because we will be interested not only in the input-output relationships of the electromagnetic fields, i.e. $A_a(0,L)$, but also evolution of noise generated at a point z that propagates to the end of the fiber, L. In the following subsections, we provide expressions for $\mu_j(z,L)$ and $\nu_j(z,L)$ for the three main cases of interest.

3.A. Distributed loss solution

In the most general case, when there are no restrictions on Δk and distributed linear loss is present, Eqs. (9–11) can be shown to have a series solution. We here briefly outline the derivation of this solution. Solving for the mean field of the pump, Eq. (9), we obtain

$$\bar{A}_p(z) = \exp[i\gamma_0 I_p(0) z_{\mathrm{eff}} - \frac{\alpha z}{2}], \tag{14}$$

where the effective length $z_{\rm eff}$ is defined to be $z_{\rm eff} = [1 - \exp(-\alpha_p z)]/\alpha_p$. Further defining the initial pump power in Watts to be $I_p(0) = |\bar{A}_p(0)|^2$, and setting the reference phase to be that of the pump at the input of the fiber, we substitute the resulting expressions into Eqs. (10) and (11). Writing

$$\bar{A}_a = \bar{B}_a \exp[i(\gamma_0 + \gamma_\Omega) I_p(0) z_{\rm eff} - \alpha_a z/2], \tag{15}$$

$$\bar{A}_s = \bar{B}_s \exp[i(\gamma_0 + \gamma_{-\Omega}) I_p(0) z_{\rm eff} - \alpha_s z/2], \tag{16}$$

and making a change of variable from z to $z_{\rm eff}$, one obtains

$$\frac{{\rm d}\bar{B}_a}{{\rm d}z_{\rm eff}} = i\gamma_\Omega I_p(0) \exp[-f(z_{\rm eff})] \bar{B}_s^*, \tag{17}$$

$$\frac{{\rm d}\bar{B}_s^*}{{\rm d}z_{\rm eff}} = -i\gamma_{-\Omega}^* I_p(0) \exp[f(z_{\rm eff})] \bar{B}_a, \tag{18}$$

where

$$f(z_{\rm eff}) = i[\gamma_\Omega + \gamma_{-\Omega}^*] I_p(0) z_{\rm eff} - \frac{(\alpha_s - \alpha_a + 2i\Delta k) \ln(1 - \alpha_p z_{\rm eff})}{2\alpha_p}. \tag{19}$$

After some algebra and making use of the substitutions

$$\bar{F}_a = \bar{B}_a \exp[f(z_{\rm eff})], \tag{20}$$

$$\bar{F}_s^* = \bar{B}_s^* \exp[-f(z_{\rm eff})], \tag{21}$$

we can obtain the nonlinear coupled equations

$$\frac{{\rm d}\bar{F}_a}{{\rm d}z_{\rm eff}} - [\Gamma + \frac{\Lambda}{1 - \alpha_p z_{\rm eff}}] \bar{F}_a = \xi_1 \bar{F}_s^*, \tag{22}$$

$$\frac{{\rm d}\bar{F}_s^*}{{\rm d}z_{\rm eff}} + [\Gamma + \frac{\Lambda}{1 - \alpha_p z_{\rm eff}}] \bar{F}_s^* = \xi_2 \bar{F}_a, \tag{23}$$

where the following constants are used for calculating evolution from point z to L: $\Gamma = i[\gamma_\Omega + \gamma_{-\Omega}^*] I_p(z)/2$, $\Lambda = [\alpha_s/2 - \alpha_a/2 + i\Delta k]/2$, $\xi_1 = i\gamma_\Omega I_p(z)$, and $\xi_2 = -i\gamma_{-\Omega}^* I_p(z)$. Using the expansion

$$\frac{1}{1 - \alpha_p z_{\rm eff}} = \sum_{n=0}^{\infty} \alpha_p^n z_{\rm eff}^n, \tag{24}$$

on the nonlinear term in Eqs. (22) and (23), we find a series solution for $\bar{F}_j$ and then obtain $\bar{A}_j$.

The series solution converges in relatively few terms when $\alpha_p z_{\rm eff}$ is small, which is the case for practical amplifiers. The following solutions are then obtained:

$$\mu_a(z, L) = \exp[p(z, L)] \sum_{n=0}^{\infty} a_n L_{\rm eff}^n \quad (a_0 = 1, s_0^* = 0), \tag{25}$$

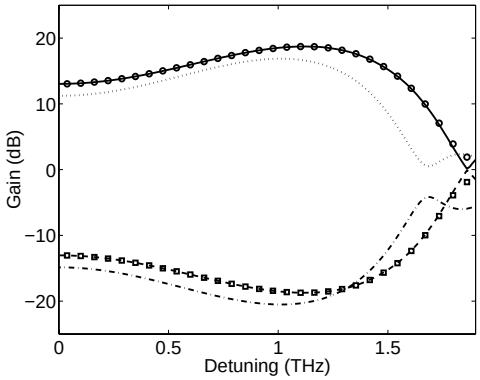

Fig. 2. Gain spectrum vs. detuning for PSA made from DSF for (a) optimum lossless PSA of fiber length $L = L_{\text{eff}} = 3.63$ km, and $\text{Im}\{\gamma_\Omega\} = 0$ (solid curve), (b) optimum lossless PSA of fiber length $L = L_{\text{eff}} = 3.63$ km, and $\text{Im}\{\gamma_\Omega\}$ calculated for DSF as explaine in the text (circles), (c) optimum PSA of fiber length $L = 4.44$ km, and thus $L_{\text{eff}} = 3.63$ km with $\alpha_a = \alpha_s = \alpha_p = 0.41$ db/km and $\text{Im}\{\gamma_\Omega\}$ calculated for DSF as explained in the text (dotted curve), (d) optimum lossless PSD of fiber length $L = L_{\text{eff}} = 3.63$ km, and $\text{Im}\{\gamma_\Omega\} = 0$ (dashed curve), (e) optimum lossless PSD of fiber length $L = L_{\text{eff}} = 3.63$ km, and $\text{Im}\{\gamma_\Omega\}$ calculated for DSF as explaine in the text (squares), (f) optimum PSD of fiber length $L = 4.44$ km, and thus $L_{\text{eff}} = 3.63$ km with $\alpha_a = \alpha_s = \alpha_p = 0.41$ db/km and $\text{Im}\{\gamma_\Omega\}$ calculated for DSF as explained in the text (dash-dotted curve). Input pump power is 0.33 Watts, $\lambda_0 = 1551.16$ nm, pump wavelength is 1551.5 nm, and the dispersion slope is 57 ps/(nm^2 km).

$$\mu_s(z,L) = \exp[p(z,L)] \sum_{n=0}^{\infty} s_n L_{\text{eff}}^n \quad (a_0 = 0, s_0^* = 1), \tag{26}$$

$$\nu_a(z,L) = \exp[p(z,L)] \sum_{n=0}^{\infty} a_n L_{\text{eff}}^n \quad (a_0 = 0, s_0^* = 1), \tag{27}$$

$$\nu_s(z,L) = \exp[p(z,L)] \sum_{n=0}^{\infty} s_n L_{\text{eff}}^n \quad (a_0 = 1, s_0^* = 0), \tag{28}$$

where

$$p(z,L) = i[\gamma_0 + (\gamma_\Omega - \gamma_{-\Omega}^*)/2] I_p(z) L_{\text{eff}} \tag{29}$$

$$-i\Delta k(L-z)/2 - \alpha_a(L-z)/4 - \alpha_s(L-z)/4 \tag{30}$$

and $L_{\text{eff}} = \{1 - \exp[-\alpha_p(L-z)]\}/\alpha_p$. The coefficients a_n and s_n^* are then calculated through

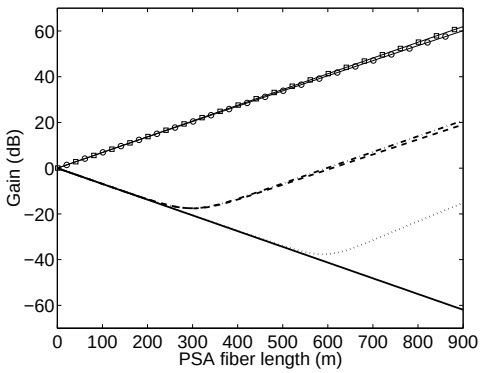

Fig. 3. Gain vs. fiber length for PSA made from DSF for (a) phase-sensitive deamplification with optimum power splitting in lossless fiber ($\alpha_a = \alpha_s = \alpha_p = 0$) (thick solid line), (b) phase-sensitive deamplification with optimum power splitting in a lossy fiber ($\alpha_a = \alpha_s = \alpha_p = 0.25$ dB/km) (dotted line), (c) phase-sensitive deamplification in a lossless fiber with $|\zeta_a|^2 = |\zeta_s|^2$ (dash-dotted line), (d) phase-sensitive deamplification in a lossy fiber with $|\zeta_a|^2 = |\zeta_s|^2$ (dashed line), (e) phase-sensitive amplification in a lossless fiber with $|\zeta_a|^2 = |\zeta_s|^2$ (squares) and optimum input power splitting (solid curve under the squares), and (f) phase-sensitive amplification in a lossy fiber with $|\zeta_a|^2 = |\zeta_s|^2$ (circles) and optimum input power splitting (solid curve under the circles). Input pump power is 4 Watts, pump-signal detuning is 1 THz, and phase-matching is achieved at the input ($\Delta k = -2\mathrm{Re}\{\gamma_\Omega\} I_p(0)$).

the following recursion relations:

$$a_n = \frac{\Gamma a_{n-1} + \xi_1 s^*_{n-1} + \Lambda \sum_{j=0}^{n-1} \alpha_p^j a_{n-1-j}}{n}, \tag{31}$$

$$s^*_n = \frac{-\Gamma s^*_{n-1} + \xi_2 a_{n-1} - \Lambda \sum_{j=0}^{n-1} \alpha_p^j s^*_{n-1-j}}{n}. \tag{32}$$

3.B. Lossless, $\Delta k \neq 0$ solution

The solution for lossless fiber and $\Delta k \neq 0$ is well known, as are the μ and ν functions which can be expressed as[35]

$$\mu_a(z,L) = \exp\left(-\frac{i\left(\Delta k - [2\gamma_0 + \gamma_\Omega - \gamma^*_{-\Omega}] I_p\right)(L-z)}{2}\right) \times \left(\frac{i\kappa}{2g}\sinh[g(L-z)] + \cosh[g(L-z)]\right), \tag{33}$$

$$\mu_s(z,L) = \exp\left(-\frac{i\left(\Delta k - [2\gamma_0 + \gamma_{-\Omega} - \gamma_{\Omega}^*]I_p\right)(L-z)}{2}\right) \left(\frac{i\kappa^*}{2g^*}\sinh[g^*(L-z)] + \cosh[g^*(L-z)]\right), \quad (34)$$

$$\nu_a(z,L) = \exp\left(-\frac{i\left(\Delta k - [2\gamma_0 + \gamma_{\Omega} - \gamma_{-\Omega}^*]I_p\right)(L-z)}{2}\right)\frac{i\gamma_{\Omega}I_p}{g}\sinh[g(L-z)], \quad (35)$$

$$\nu_s(z,L) = \exp\left(-\frac{i\left(\Delta k - [2\gamma_0 + \gamma_{-\Omega} - \gamma_{\Omega}^*]I_p\right)(L-z)}{2}\right)\frac{i\gamma_{-\Omega}I_p(z)}{g^*}\sinh[g^*(L-z)]. \quad (36)$$

Here $I_p(z) = I_p = |\bar{A}_p(0)|^2$ is the pump power in Watts, $\kappa = \Delta k + (\gamma_{\Omega} + \gamma_{-\Omega}^*)I_p$, and $g = \sqrt{-(\kappa/2)^2 + \gamma_{\Omega}\gamma_{-\Omega}^* I_p^2}$ is the complex gain coefficient.

3.C. Lossless, $\Delta k = 0$ solution

We also state the results for the lossless, $\Delta k = 0$ case, which is useful in our analysis near degeneracy. We have $\Delta k = 0$ when the FOPA is pumped at the zero dispersion wavelength or if the system is treated as if dispersionless. When the three frequencies are very nearly degenerate, we can also make the approximation that $\Delta k = 0$. Then the μ and ν functions become

$$\mu_a(z,L) = \exp\left[i\left(\frac{2\gamma_0 + \gamma_{\Omega} - \gamma_{-\Omega}^*}{2}\right)I_p(L-z)\right][1 + i\gamma_{\Omega}I_p(L-z)], \quad (37)$$

$$\mu_s(z,L) = \exp\left[i\left(\frac{2\gamma_0 + \gamma_{-\Omega} - \gamma_{\Omega}^*}{2}\right)I_p(L-z)\right][1 + i\gamma_{-\Omega}I_p(L-z)], \quad (38)$$

$$\nu_a(z,L) = \exp\left[i\left(\frac{2\gamma_0 + \gamma_{\Omega} - \gamma_{-\Omega}^*}{2}\right)I_p(L-z)\right]i\gamma_{\Omega}I_p(L-z), \quad (39)$$

$$\nu_s(z,L) = \exp\left[i\left(\frac{2\gamma_0 + \gamma_{-\Omega} - \gamma_{\Omega}^*}{2}\right)I_p(L-z)\right]i\gamma_{-\Omega}I_p(L-z). \quad (40)$$

Under the normal assumption of an anti-symmetric Raman gain profile ($\gamma_{\Omega} = \gamma_{-\Omega}^*$), we see the power gain, $G = |\mu_a(0,L)|^2 = 1 + 2\mathrm{Im}\{\gamma_{\Omega}\}I_pL + |\gamma_{\Omega}|^2 I_p^2 L^2$, has a four wave mixing gain that is quadratic as a function of fiber length and that the Raman loss at the anti-Stokes wavelength is linear in pump power and length ($2\mathrm{Im}\{\gamma_{\Omega}\}I_pL$). Similarly, the Raman gain at the Stokes wavelength is linear in power and length ($2\mathrm{Im}\{\gamma_{-\Omega}\}I_pL$).

3.D. Optimal classical phase-sensitive amplification and deamplification

We next find the optimal phase-sensitive amplification and phase-sensitive deamplification of a mean field consisting of a superposition of Stokes and anti-Stokes fields. We define optimal phase-sensitive amplification (deamplification) as the greatest (least) output signal power

possible for a fixed amount of input signal power. Assuming coherent signal inputs ζ_j having powers $|\zeta_j|^2$ and phases $\exp(i\theta_j)$ for $j = a, s$, the phase-sensitive gain of the PSA is

$$\begin{aligned} G &= \frac{|\bar{A}_a(L)|^2 + |\bar{A}_s(L)|^2}{|\bar{A}_a(0)|^2 + |\bar{A}_s(0)}|^2 \\ &= \frac{|\mu_a\zeta_a + \nu_a\zeta_s^*|^2 + |\mu_s\zeta_s + \nu_s\zeta_a^*|^2}{|\zeta_a|^2 + |\zeta_s|^2} \\ &= \frac{(|\mu_a|^2 + |\nu_s|^2)|\zeta_a|^2 + (|\nu_a|^2 + |\mu_s|^2)|\zeta_s|^2 + \left\{[(\mu_s\nu_s^* + \mu_a\nu_a^*)|\zeta_a||\zeta_s|\ e^{i(\theta_a+\theta_s)}] + \text{c.c.}\right\}}{|\zeta_a|^2 + |\zeta_s|^2}. \end{aligned} \tag{41}$$

By properly choosing the relative power of the Stokes and anti-Stokes inputs and their sum phase $\theta = \theta_a + \theta_s$ relative to the input pump phase, one achieves maximimum (minimimum) phase-sensitive amplification (deamplification). The optimum sum phases $\theta_{\text{psa, opt}}$ and $\theta_{\text{psd, opt}}$ are

$$\theta_{\text{psa, opt}} = -\arg[\mu_s\nu_s^* + \mu_a\nu_a^*], \tag{42}$$

$$\theta_{\text{psd, opt}} = \pi - \arg[\mu_s\nu_s^* + \mu_a\nu_a^*], \tag{43}$$

for amplification and deamplification, respectively. By setting the sum input power $|\zeta_a|^2 + |\zeta_s|^2 = \mathcal{C}$ to be some constant $\mathcal{C}$, the extrema of Eq. (41) can be found to occur when the proportion of input anti-Stokes power to the total input power is

$$\frac{|\zeta_a|^2}{|\zeta_a|^2 + |\zeta_s|^2} = \frac{1}{2}\left(1 \pm \frac{|\mu_s|^2 - |\mu_a|^2}{\sqrt{4|\mu_a\nu_a^* + \mu_s\nu_s^*|^2 + [|\mu_s|^2 - |\mu_a|^2]^2}}\right) \tag{44}$$

where the negative root corresponds to optimum phase-sensitive amplification, the positive root to optimum phase-sensitive deamplification. The maximum PSA gain, G_{PSA} is found by insertion of Eqs. (42) and (44) into Eq. (41). The result simplifies to:

$$\begin{aligned} G_{\text{PSA}} &= \frac{(|\mu_a|^2 + |\mu_s|^2 + |\nu_a|^2 + |\nu_s|^2)}{2} + \frac{\sqrt{4|\mu_a\nu_a^* + \mu_s\nu_s^*|^2 + (|\mu_s|^2 - |\mu_a|^2)^2}}{2} \\ &\quad + \frac{(|\mu_s|^2 - |\mu_a|^2)(|\nu_a|^2 - |\nu_s|^2)}{\sqrt{4|\mu_a\nu_a^* + \mu_s\nu_s^*|^2 + (|\mu_s|^2 - |\mu_a|^2)^2}}. \end{aligned} \tag{45}$$

In Fig. 2 all of the plots are optimal in the sense that the best total phase and relative power of the input fields is chosen. It is clear that the Raman effect is negligible as those curves including the Raman effect (circles and squares) are very similar to those neglecting it (solid curve and dashed curve). This plot shows also that the definition of the effective length is a mathematical one and not a good guide for estimating the gain profile. The dotted and dash-dot curves show the gain spectrum of a lossy fiber (0.41 db/km) 4.44 km in length.

The other curves are for a lossless fiber of the effective length $L_{\rm eff} = 3.63$ km in length. Thus distributed loss has a greater effect than might be supposed: fibers experience noticeably less gain than lossless fibers do when the lossless fiber has a length equal to the effective length of a lossy fiber fiber.

Some of the characteristics of the classical phase-sensitive response can be seen in Fig. 3, which is a plot of the phase-sensitive gain vs. fiber length. The primary feature of phase-sensitive amplification is that the mean field gain is relatively insensitive to the relative strength of the two input fields (this can be seen by the overlap of the thin solid lines with the squares and circles. In addition, typical distributed losses do not significantly impact the gain of the fiber, as can be seen by comparison of the squares (lossless fiber) with the circles, which represent fiber with loss of 0.25 db/km. On the other hand, the achievable degree of phase-sensitive deamplification is much more sensitive to the relative proportion of the input fields which can be seen by comparison of the dash-dotted and dashed lines (equal power splitting, i.e. $|\zeta_a|^2 = |\zeta_s|^2$) with the dotted and thick solid lines (optimum relative proportion). In addition, distributed losses also set a limit on classical deamplification as can be seen by comparison of the dashed line (lossy) with the dash-dotted lines (lossless) and comparison of the dotted line (lossy) with the thick solid line (lossless).

4. Input-output quantum mode transformations

In this section, we discuss the quantum mechanics of the $\chi^{(3)}$ parametric amplifier and derive input-output mode transformations in the Heisenberg picture which can be used to calculate the noise figure of the phase-sensitive operation of a FOPA and the accompanying quadrature squeezing. Here we also extend our previously described quantum theory[10,11] to include the effects of loss.

Consider the field operator

$$\hat{A}(t) = \hat{A}_p + \hat{A}_s \exp(i\Omega t) + \hat{A}_a \exp(-i\Omega t) \tag{46}$$

for the total field propagating through a FOPA having a frequency and polarization degenerate pump. The quantum equation of motion for the total field is like that in Boivin,[27] which is derived in detail in Kärtner[28]):

$$\begin{aligned} \frac{\partial \hat{A}(t)}{\partial z} &= -\int \frac{\alpha(\Omega)}{2} \widetilde{\hat{A}}(\Omega) \exp(i\Omega t)\, \mathrm{d}\Omega + i \left[\int \mathrm{d}\tau\, h(t-\tau) \hat{A}^\dagger(\tau) \hat{A}(\tau) \right] \hat{A}(t) \\ &+ i\, \hat{m}(z,t) \hat{A}(t) \end{aligned} \tag{47}$$

wherein $h(t)$ is the causal response function of the nonlinearity; i.e., the inverse Fourier transform of $H(\Omega)$ in Eq. (4). In Eq. (47), $\hat{m}(z,t)$ is a Hermitian phase-noise operator

$$\hat{m}(z,t) = \int_0^\infty \mathrm{d}\Omega\, \frac{\sqrt{W(\Omega)}}{2\pi} \{ i\, \hat{d}_\Omega^\dagger(z) e^{i\,\Omega t} - i\, \hat{d}_\Omega(z) e^{-i\Omega t} \}, \tag{48}$$

which describes coupling of the field to a collection of localized, independent, medium oscillators (optical phonon modes), and $\alpha_\Omega \hat{v}_\Omega(z,t)$ describes the coupling of the field to a collection of localized, independent, oscillators in vacuum state. This coupling is required to preserve the continuous-time commutators

$$[\hat{A}(t), \hat{A}^\dagger(t')] = \delta(t-t'), \tag{49}$$

$$[\hat{A}(t), \hat{A}(t')] = 0. \tag{50}$$

Note that the time t is in a reference frame traveling at group velocity v_g, i.e., $t = t_{\text{stationary frame}} - \frac{z}{v_g}$. The weighting function $W(\Omega)$ must be positive for $\Omega > 0$ so that the molecular vibration oscillators absorb energy from the mean fields rather than providing energy to the mean fields. The operators $\hat{d}_\Omega(z)$ and $\hat{d}^\dagger_\Omega(z)$ obey the commutation relation

$$[\hat{d}_\Omega(z), \hat{d}^\dagger_{\Omega'}(z')] = \delta(\Omega - \Omega')\delta(z-z') \tag{51}$$

and each phonon mode is in thermal equilibrium:

$$\langle \hat{d}^\dagger_\Omega(z) \hat{d}_{\Omega'}(z') \rangle = \delta(\Omega - \Omega')\delta(z-z') n_{\text{th}} \tag{52}$$

with a mean phonon number $n_{\text{th}} = [\exp(\hbar\Omega/kT) - 1]^{-1}$. Here $\hbar$ is Planck's constant over 2π, k is Boltzmann's constant, and T is the temperature. Looking ahead to a Fourier domain treatment of the parametric amplifier, note that the creation operator at each Ω, $\hat{d}^\dagger_\Omega(z)$, oscillates as $e^{i\Omega t}$ (a Stokes detuning frequency) and that the annihilation operator at each Ω, $\hat{d}_\Omega(z)$, oscillates as $e^{-i\Omega t}$ (an anti-Stokes detuning frequency).

In what follows, gain and quantum fluctuations occur at a point z in the fiber and it is necessary to solve for the total field and fluctuations at the output point L.

The pump, Stokes, and anti-Stokes fields are treated as separate frequency modes, implying that the required commutators are

$$[\hat{A}_j(z), \hat{A}^\dagger_k(z')] = \delta_{jk}\delta(z-z'), \tag{53}$$

$$[\hat{A}_j(z), \hat{A}_k(z')] = 0, \tag{54}$$

for $j, k \in \{p, a, s\}$.

Linearization of the Fourier transformation of Eq. (47) shows that the quantum fluctuations of the pump contribute negligibly small amounts of fluctuations to the Stokes and anti-Stokes waves when the pump is strong. These fluctuations are neglected by replacing the pump field operators with their mean fields. Under the strong pump approximation it is also acceptable to neglect the fluctuation operators at all frequencies except the Stokes and anti-Stokes frequencies because the pump mean-field will interact only with these modes of

interest to a non-negligible degree, as is also shown by linearization of the quantum fluctuations around the mean fields. As a result, we obtain

$$\frac{\mathrm{d}\bar{A}_p}{\mathrm{d}z} = i\,\gamma_0\,|\bar{A}_p|^2\bar{A}_p - \frac{\alpha_p}{2}\bar{A}_p, \tag{55}$$

$$\begin{aligned}\frac{\mathrm{d}\hat{A}_a}{\mathrm{d}z} &= i\,(\gamma_0+\gamma_\Omega)\,|\bar{A}_p|^2\hat{A}_a + i\gamma_\Omega\bar{A}_p^2\hat{A}_s^\dagger\exp\left(-i\Delta k z\right) - \alpha_a\hat{A}_a \\ &\quad +\sqrt{2\mathrm{Im}\{\gamma_\Omega\}}\hat{d}_\Omega(z)\bar{A}_p\exp[i(k_p-k_a)z] + \sqrt{\alpha_a}\hat{A}_a(z),\end{aligned} \tag{56}$$

$$\begin{aligned}\frac{\mathrm{d}\hat{A}_s}{\mathrm{d}z} &= i\,(\gamma_0+\gamma_{-\Omega})\,|\bar{A}_p|^2\hat{A}_s + i\gamma_{-\Omega}\bar{A}_p^2\hat{A}_a^\dagger\exp\left(-i\Delta k z\right) \\ &\quad -\sqrt{2\mathrm{Im}\{\gamma_{-\Omega}\}}\hat{d}_\Omega^\dagger(z)\bar{A}_p\exp[i(k_p-k_s)z] + \sqrt{\alpha_s}\hat{A}_s(z),\end{aligned} \tag{57}$$

Under the undepleted pump approximation, wherein the pump is treated essentially classically, it is also permissible to relax the commutation relations so that only the commutators at Stokes and anti-Stokes frequencies are required to be preserved. Even when the pump is treated quantum mechanically, changes to the commutatators of the pump field are of second order in this linearized first-order theory. Therefore the commutators that are required to be obeyed are:

$$[\hat{A}_j(z), \hat{A}_k^\dagger(z')] = \delta_{jk}\delta(z-z'), \tag{58}$$

$$[\hat{A}_j(z), \hat{A}_k(z')] = 0, \tag{59}$$

for $j,k = a,s$ only.

The solution of Eqs. (56) and (57) is

$$\begin{aligned}\hat{A}_a(L) &= \mu_a(0,L)\hat{A}_a(0) + \nu_a(0,L)\hat{A}_s^\dagger(0) + \\ &\quad \sqrt{2\mathrm{Im}\{\gamma_\Omega\}}\int_0^L \mathrm{d}z\,\bar{A}_p(z)\exp[i(k_p-k_a)z]\,[\mu_a(z,L)-\nu_a(z,L)]\,\hat{d}_\Omega(z), \\ &\quad +\int_0^L \mathrm{d}z\,[\sqrt{\alpha_a}\mu_a(z,L)\hat{v}_a(z) + \sqrt{\alpha_s}\nu_a(z,L)\hat{v}_s^\dagger(z)]\end{aligned} \tag{60}$$

$$\begin{aligned}\hat{A}_s(L) &= \mu_s(0,L)\hat{A}_s(0) + \nu_s(0,L)\hat{A}_a^\dagger(0) + \\ &\quad \sqrt{2\mathrm{Im}\{\gamma_\Omega\}}\int_0^L \mathrm{d}z\,\bar{A}_p(z)\exp[i(k_p-k_s)z]\,[-\mu_s(z,L)+\nu_s(z,L)]\,\hat{d}_\Omega^\dagger(z). \\ &\quad +\int_0^L \mathrm{d}z\,[\sqrt{\alpha_s}\mu_s(z,L)\hat{v}_s(z) + \sqrt{\alpha_a}\nu_s(z,L)\hat{v}_a^\dagger(z)]\end{aligned} \tag{61}$$

In the notation used in this paper, the functions $\mu_j(z,L)$ and $\nu_j(L,z)$ denote evolution from a point z in the fiber to the end of the fiber (L) where the intensity and phase of the pump at point z must be used.

In this section, we have presented a thorough derivation of the input-output mode transformations that govern a lossless $\chi^{(3)}$ parametric amplifier. In the following two sections, we use these input-output mode transformations to obtain the noise figure of $\chi^{(3)}$ phase-sensitive parametric amplifiers and the squeezing parameter for quadrature squeezing.

5. Noise Figure of phase-sensitive amplification

In this section we discuss the noise figure of phase-sensitive amplification, which is defined as

$$\mathrm{NF} = \frac{\mathrm{SNR}_{\mathrm{in}}}{\mathrm{SNR}_{\mathrm{out}}}. \tag{62}$$

We assume for our treatment here that the difference between the Stokes and anti-Stokes frequencies exceeds the bandwidth of the detector. Thus beat frequencies of these two waves will not be detected and can be neglected. The input power at the Stokes and anti-Stokes wavelength is $\langle \hat{A}_j^\dagger(0)\hat{A}_j(0)\rangle = |\zeta_j|^2$, which has units of Watts, and is assumed to be in a coherent state having mean photon number $\langle \hat{n}_j\rangle = \langle \hat{A}_j^\dagger(0)\hat{A}_j(0)\rangle/(\hbar\omega_j) = |\zeta_j|^2/(\hbar\omega_j)$. In what follows, we neglect the small frequency difference between ω_a and ω_s. Thus the input SNR can be written as

$$\mathrm{SNR}_{\mathrm{in}} = \frac{(\langle \hat{n}_a\rangle + \langle \hat{n}_s\rangle)^2}{\langle \Delta\hat{n}_a\rangle + \langle \Delta\hat{n}_s\rangle} = \frac{(|\zeta_a|^2 + |\zeta_s|^2)^2}{|\zeta_a|^2 + |\zeta_s|^2} = |\zeta_a|^2 + |\zeta_s|^2. \tag{63}$$

Calculating the output SNR in a similar way and plugging into Eq. (62), the NF for phase-sensitive amplification can be expressed as

$$\mathrm{NF} = \frac{(|\zeta_a|^2 + |\zeta_s|^2)(\langle \Delta\hat{n}^2_{\mathrm{PI}}\rangle + \langle \Delta\hat{n}^2_{\mathrm{PS}}\rangle)}{(P_a + P_s)^2}, \tag{64}$$

where the mean output power at each wavelength, P_a and P_s, is

$$P_a = |\mu_a|^2|\zeta_a|^2 + |\nu_a|^2|\zeta_s|^2 + (\zeta_a\zeta_s\mu_a\nu_a^* + \mathrm{c.c.}), \tag{65}$$

$$P_s = |\mu_s|^2|\zeta_s|^2 + |\nu_s|^2|\zeta_a|^2 + (\zeta_a\zeta_s\mu_s\nu_s^* + \mathrm{c.c.}). \tag{66}$$

In Eq. (64), we have expressed the variance of the output photocurrent as the sum of a phase-insensitive portion, $\langle \Delta\hat{n}^2_{\mathrm{PI}}\rangle$, and a phase-sensitive portion, $\langle \Delta\hat{n}^2_{\mathrm{PS}}\rangle$, which are calculated to be

$$\langle \Delta\hat{n}^2_{\mathrm{PI}}\rangle = P_aB_a + P_sB_s, \tag{67}$$

$$\langle \Delta\hat{n}^2_{\mathrm{PS}}\rangle = 2Q^*B_1 + 2QB_2, \tag{68}$$

where the quantities

$$B_j = |\mu_j|^2 + |\nu_j|^2 + (2n_{\mathrm{th}} + 1)|r_j|^2 + |c_{j1}|^2 + |c_{j2}|^2, \quad (j = a, s) \tag{69}$$

$$Q = (\mu_a\zeta_a + \nu_a\zeta_s^*)(\mu_s\zeta_s + \nu_s\zeta_a^*) \tag{70}$$

$$B_1 = c_{x1} + r_x(n_{\mathrm{th}} + 1) + \mu_a\nu_s, \tag{71}$$

$$B_2 = c_{x2}^* + r_x^*n_{\mathrm{th}} + \mu_s^*\nu_a^*, \tag{72}$$

which have noise terms defined as follows:

$$|r_a|^2 = 2\mathrm{Im}\{\gamma_\Omega\}\int_0^L \mathrm{d}z\,|\bar{A}_p(z)|^2|\mu_a(z,L)-\nu_a(z,L)|^2, \tag{73}$$

$$|r_s|^2 = -2\mathrm{Im}\{\gamma_{-\Omega}\}\int_0^L \mathrm{d}z\,|\bar{A}_p(z)|^2|\mu_s(z,L)-\nu_s(z,L)|^2, \tag{74}$$

$$|c_{a(s)1}|^2 = \int_0^L \mathrm{d}z\,\alpha_{a(s)}|\mu_{a(s)}(z,L)|^2, \tag{75}$$

$$|c_{a(s)2}|^2 = \int_0^L \mathrm{d}z\,\alpha_{s(a)}|\nu_{a(s)}(z,L)|^2, \tag{76}$$

$$\begin{aligned} r_x = {} & 2\mathrm{Im}\{\gamma_\Omega\}\int_0^L \mathrm{d}z\,\bar{A}_p^2(z)\exp(-i\Delta k z) \\ & \times[\mu_a(z,L)-\nu_a(z,L)][-\mu_s(z,L)+\nu_s(z,L)], \end{aligned} \tag{77}$$

$$c_{x1} = \alpha_a\int_0^L \mathrm{d}z\,\mu_a(z,L)\nu_s(z,L), \tag{78}$$

$$c_{x2}^* = \alpha_s\int_0^L \mathrm{d}z\,\nu_a(z,L)^*\mu_s(z,L)^*. \tag{79}$$

In the above expressions, $|r_{a(s)}|^2$ represents the integrated amplified noise at the anti-Stokes (Stokes) wavelength seeded by thermally populated optical phonon modes that are coupled in by the Raman process. The terms $|c_{a(s)1}|^2$ represent integrated amplified noise at the anti-Stokes (Stokes) wavelength seeded by vacuum noise mixed in through distributed loss at the anti-Stokes (Stokes) wavelength, while the terms $|c_{a(s)2}|^2$ represent amplified noise at the anti-Stokes (Stokes) wavelength seeded by vacuum noise mixed in through distributed loss at the Stokes (anti-Stokes) wavelength.

In addition, the phase-sensitive terms $\mu_a\nu_s$ and $\mu_s^*\nu_a^*$ represent amplified phase-sensitive noise seeded by the vacuum noise at the anti-Stokes and Stokes wavelengths. The quantity r_x represents amplified phase-sensitive noise seeded by the thermal-phonon fields due the Raman effect, and c_{x1} and c_{x2} represent the amplified phase-sensitive noise seeded by the vacuum noise due to distributed linear losses. Phase-sensitive noise is present when the photocurrent variance with both Stokes and anti-Stokes waves impinging on a detector is different from the sum of the individual noise variances of the Stokes and anti-Stokes frequency.

5.A. Degenerate Limit

By taking the limiting value of the NF as $\Omega \to 0$, we find the NF performance of a fully degenerate FOPA. We find this limiting value of the NF by expanding the anti-symmetric imaginary part of γ_Ω in a Taylor seris and expanding the exponential in $n_{th} = \{\exp[\hbar\Omega/(kT)]-1\}^{-1}$ before allowing $\Omega \to 0$. We also use the fact that in this limit, Δk also approaches 0 and the optimum power splitting ratio approaches 0.5. This NF limit is:

$$NF_{\mathrm{PSA},\,\Omega\to 0} = 1 + \frac{\frac{4kT\gamma_i'(0)}{\hbar\gamma_0}\left[1-\frac{\phi_{\mathrm{NL}}}{\sqrt{1+\phi_{\mathrm{NL}}^2}}\right]}{1+2\phi_{\mathrm{NL}}^2+2\phi_{\mathrm{NL}}\sqrt{1+\phi_{\mathrm{NL}}^2}}, \tag{80}$$

where $\phi_{\rm NL} = \gamma_0 I_p(0) L$ is the nonlinear phase shift and $\gamma_i'(0)$ is the slope of the imaginary part of γ_Ω as $\Omega \to 0$. We observe that the PSA noise figure increases to a maximum of slightly more than 0 dB then decreases again and approaches 0 dB in the high gain limit. This unusual decreasing noise figure vs. nonlinear phase shift is due to the relative scaling of the Raman and FWM processes when $\Delta k = 0$ and the mean Raman gain of the Stokes and anti-Stokes wavelengths vanishes. Then Raman noise scales linearly, and in addition the Raman noise entering at the Stokes and anti-Stokes frequencies does not undergo further amplification. The signal, however, undergoes quadratic gain so that the Raman noise contribution to the NF becomes negligible.

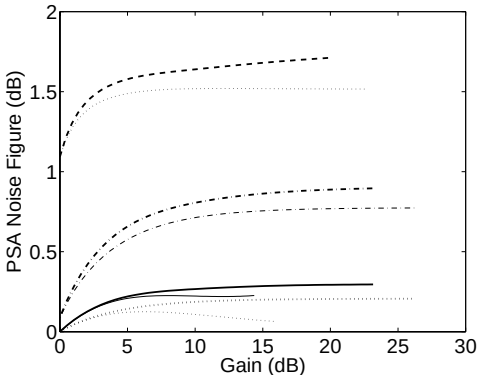

Fig. 4. PSA noise figure vs. Gain for various detunings. For thick lines, attenuation is 0.75 dB/km at pump, Stokes, and anti-Stokes wavelengths; for thin lines, fiber is lossless. $\Omega/2\pi$ = 13.8 THz, dashed curves; $\Omega/2\pi$ = 1.38 THz, dash-dotted curves; $\Omega/2\pi$ = 40 GHz, solid curves; and $\Omega/2\pi$ = 0 Hz, dotted curves. Except for dotted curves, phase matching at the input ($\Delta k = -2\mathrm{Re}\{\gamma_\Omega\} I_p(0)$) is achieved. For dotted, $\Delta k = 0$. The relative phase and power splitting at the input is for optimal classical gain. Initial pump power is 340 mW, $\gamma(0)$ = 9E−3 $\mathrm{W}^{-1}\mathrm{m}^{-1}$, peak imaginary part of $\gamma(\Omega)$ is 3.5E−3 $\mathrm{W}^{-1}\mathrm{m}^{-1}$. Fiber length is 1 km.

In Fig. 4, we plot the noise figure vs. PSA gain for several values of detuning for a typical highly-nonlinear fiber with a loss coefficient of 0.75 dB/km. The results show that for detunings achievable by use of electrooptic elements (40 GHz detuning, dash-dotted curve), results are almost exactly the same as would be achieved in the limit of zero detuning (curve marked with x). For this simulation, we use realistic values for $\gamma(0)$ and for the distributed loss. We have additionally assumed that the highly nonlinear fiber has the same ratio of $\mathrm{Im}\{\gamma(\Omega)\}$ to $\mathrm{Re}\{\gamma(\Omega)\}$ as dispersion shifted fiber, i.e., the two have the same germanium content.

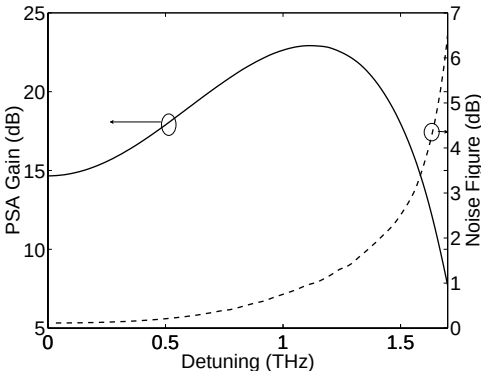

Fig. 5. PSA gain and noise figure spectrum vs. detuning. Relative phase and input power splitting is for optimal classical gain. Initial pump power is 300 mW, $\gamma(0) = 2\text{E}{-}3\ \text{W}^{-1}\text{m}^{-1}$, peak imaginary part of $\gamma(\Omega)$ is $0.75\text{E}{-}3\ \text{W}^{-1}\text{m}^{-1}$. Attenuation is 0.41 dB at pumps, Stokes, and anti-Stokes wavelengths. Fiber length is 4 km. $\lambda_0 = 1551.15$ nm, $\lambda_p = 1555.5$ nm, and dispersion slope is 57 ps/nm/km^2

Interestingly, unlike the PIA case, Fig. 4 shows that the PSA noise figure is greater than 0 dB as the gain approaches 0 dB. This occurs because the Raman gain and loss process dominates in the early parts of the amplifier (Raman gain and loss are linear in the early parts of the amplifier while four-wave-mixing gain is quadratic), adding noise to both frequencies, while the mean field undergoes no net gain due to Raman loss at one frequency and Raman gain at the other.

In Fig. 5, we show the gain and noise-figure spectrum for a 4 km fiber with fiber parameters as described in the caption. This plot shows that the increasing Raman gain coefficient with detuning causes an increased noise figure. These results show that for realistic optical fibers, a FOPA operated as a PSA can achieve a noise figure below 1 dB for detunings up to a THz.

6. Nondegenerate quadrature squeezing

When no light is injected into the FOPA, the quantum correlations between the Stokes and anti-Stokes modes imply the presence of quadrature squeezing measurable by homodyne detection with a two-frequency local oscillator (LO).

The difference current of the homodyne detector may be written as

$$\hat{I} = \hat{b}_a^\dagger \hat{q}_a + \hat{b}_s^\dagger \hat{q}_s + \text{H.c.}, \tag{81}$$

where H.c. stands for the Hermitian conjugate of the first two terms, $\hat{q}_a$ and $\hat{q}_s$ are the annihilation operators corresponding to the anti-Stokes and Stokes components of the LO

beams, which are in a coherent state with powers $|\alpha_{\mathrm{LO},j}|^2$ and relative intensities

$$y_j = \frac{|\alpha_{\mathrm{LO},j}|^2}{|\alpha_{\mathrm{LO},a}|^2 + |\alpha_{\mathrm{LO},s}|^2} \tag{82}$$

for $j = a, s$.

The squeezing parameter is defined as the ratio of the photocurrent variance with the pump on to the photocurrent variance with vacuum input entering the homodyne detector (i.e., pump off).

6.A. Lossless fiber with Raman effect

In this subsection, we concentrate on the case of a lossless FOPA. This is because increased nonlinear drive will, theoretically at least, overpower linear loss, leading to no hard limit on the achievable squeezing. However, as the Raman effect at each z scales with pump intensity as does the four-wave-mixing process, the lossless case illustrates a fundamental limit on the achievable squeezing. Using Eqs. (81) and (82), we obtain after some simple algebra for the lossless Raman-active case:

$$\begin{aligned} S(\theta, R) &= \frac{\langle \Delta \hat{I}^2 \rangle}{\langle \Delta \hat{I}^2 \rangle_{\mathrm{vac}}} \\ &= [1 + 2(|\nu_a|^2 + |r_a|^2 n_{\mathrm{th}})] y_a + \{1 + 2[|\nu_s|^2 + |r_s|^2 (1 + n_{\mathrm{th}})]\} y_s \\ &\quad + 2\{[\mu_s \nu_a (1 + n_{\mathrm{th}}) - \mu_a \nu_s n_{\mathrm{th}}] \exp[-i(\theta_a + \theta_s)] + \mathrm{c.c.}\} \sqrt{y_a y_s}. \end{aligned} \tag{83}$$

In order to produce the best squeezing, one must choose the best phase and relative intensity. Once again, these two choices are independent. In order to choose the LO phases, we note that the third term in Eq. (83) has a negative sign when

$$\theta = \pi + \arg[\mu_s \nu_a (1 + n_{\mathrm{th}}) - \mu_a \nu_s n_{\mathrm{th}}]. \tag{84}$$

Since the total LO power is conserved ($y_a + y_s = 1$), we may use this fact to eliminate y_s in Eq. (83), which then becomes quadratic in y_a. Maximizing the magnitude of the third term in Eq. (83) as a function of y_a yields the additional condition that for maximal squeezing,

$$y_a = \frac{1}{2}\left[1 + \frac{|r_s|^2(1 + n_{\mathrm{th}}) - |r_a|^2 n_{\mathrm{th}}}{\sqrt{4|\mu_s \nu_a (1 + n_{\mathrm{th}}) - \mu_a \nu_s n_{\mathrm{th}}|^2 + [|r_s|^2 (n_{\mathrm{th}} + 1) - |r_a|^2 n_{\mathrm{th}}]^2}}\right]. \tag{85}$$

Thus the power splitting of the LOs for maximal squeezing is slightly different from 50% and also slightly different from that for maximal classical deamplification.

Use of this optimal two-frequency LO yields the following optimal squeezing result

$$\begin{aligned} S_{opt} &= 1 + |\nu_a|^2 + |\nu_s|^2 + |r_a|^2 n_{\mathrm{th}} + |r_s|^2 (n_{\mathrm{th}} + 1) \\ &\quad - \sqrt{4|\mu_s \nu_a (1 + n_{\mathrm{th}}) - \mu_a \nu_s n_{\mathrm{th}}|^2 + [|r_s|^2 (1 + n_{\mathrm{th}}) - |r_a|^2 n_{\mathrm{th}}]^2}. \end{aligned} \tag{86}$$

In order to make a connection with previous work, we show that in the limit of degenerate operation we reach the same result as obtained by Shapiro.[26] By placing the pump at the zero dispersion wavelength of the fiber, our solutions are then identical to those in a dispersionless fiber (assuming the higher-order terms in an expansion of β are negligible). We thus use the expressions in Eqs. (37) to (40) for μ_j and ν_j. In order to evaluate the limit as the detuning approaches zero, we expand the anti-symmetric imaginary part of γ_Ω as an odd power series around $\Omega = 0$ and take the Taylor series expansion of the exponential in $n_{\rm th} = 1/[\exp(\hbar\Omega/(KT)) - 1]$. Then taking the limit as $\Omega \to 0$, the squeezing approaches the limit derived by Shapiro[26] for the fully degenerate case. This limit is

$$\begin{aligned} S_{opt}(0) &= 1 + 2\phi_{\rm NL}\left[\phi_{\rm NL} + \frac{2kT\gamma_i'(0)}{\hbar\gamma_0}\right] \\ &\quad -2\phi_{\rm NL}\left\{1 + \left[\phi_{\rm NL} + \frac{2kT\gamma_i'(0)}{\hbar\gamma_0}\right]^2\right\}^{1/2}, \end{aligned} \tag{87}$$

where $\phi_{\rm NL} = \gamma_0 I_p(0)L$ is the nonlinear phase shift and $\gamma_i'(0)$ is the slope of the imaginary part of γ_Ω as $\Omega \to 0$.

In Fig 6, the main features of this squeezing theory are illustrated for a lossless fiber. First, it is clear that the Raman effect degrades the achievable amount of squeezing. In addition, it can be seen by comparing dashed lines (phase-matched), dash-dotted lines (partially phase-matched) and other lines ($\Delta k = 0$) that when the Raman effect is included, phase-matching leads to worse squeezing instead of the improved squeezing predicted by an instantaneous nonlinearity model. Finally, by comparing the Raman-included dashed and dash-dotted lines, we see that when $\Delta k \neq 0$ precise balancing of the relative power splitting of the two LO frequencies is required. When this optimum splitting is achieved, the squeezing can be seen to approach a constant value. However, when $\Delta k = 0$, the possible amount of squeezing is not bounded, and squeezing asymtotically scales as $1/\phi_{\rm NL}$, which is explained by the quadratic scaling for the four-wave-mixing process and the linear scaling of the Raman process. The hard limit in the $\Delta k \neq 0$ case is caused by the fact that the four-wave-mixing and Raman effect both scale exponentially.

7. Conclusion

In conclusion, we have presented a quantum theory of parametric amplification in a $\chi^{(3)}$ nonlinear medium that includes the noninstantaneous response of the nonlinearity and the effect of distributed linear loss. We have analyzed this theory for nondegenerate phase-sensitive amplification and deamplification and have found the input conditions for optimal amplification and deamplification. We have also found the input conditions for operation with a minimum noise figure, which is predicted to be in the range of 0.4 dB in the high

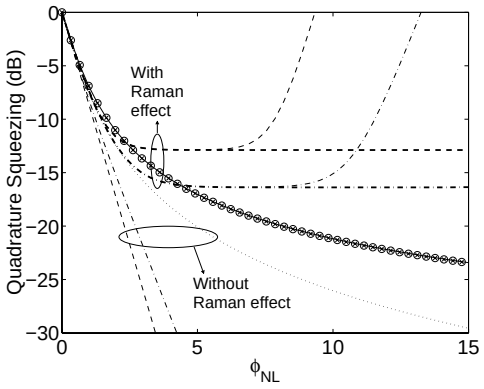

Fig. 6. Squeezing vs. nonlinear phase shift in a lossless fiber. Lower lines without Raman effect. Upper lines with Raman effect. Dashed lines signify phase-matching is achieved at the input ($\Delta k = -2\mathrm{Re}\{\gamma_\Omega\} I_p(0)$). The thick dashed line is for optimal LO power splitting, thin dashed lines for equal LO power splitting. Dash-dotted lines are for $\Delta k = -2/3\mathrm{Re}\{\gamma_\Omega\} I_p(0)$. Thick dash-dotted line is for optimal LO power splitting, thin dashed lines for equal LO power splitting. In all other lines, $\Delta k = 0$. Raman effect neglected, dotted line; Raman effect included and equal LO power splitting, marked with x; Raman effect included and optimal LO power splitting, circles; CW limit of Eq. (87) with $\gamma_i^{'}(0) kT/\hbar\gamma_0 = 0.026$. Pump-signal detuning is 40 GHz.

gain limit with FOPAs made from typical dispersion-shifted optical fibers. We anticipate that nondegenerate phase-sensitive amplifiers will produce record noise-figure performance, as they allow circumvention of GAWBS noise that is present in the degenerate case. We have also presented a theory of non-degenerate squeezing and found the optimal continuous-wave local oscillator for a lossless FOPA having a non-instantaneous nonlinear response. We found agreement with the limit found by Shapiro as degeneracy is reached. Away from degeneracy and with a nonzero linear phase mismatch, we have shown that optimal squeezing in a dispersive fiber when $\Delta k \neq 0$ will reach a constant limit, unlike the $1/\phi_{\mathrm{nl}}$ scaling that occurs when the linear phase mismatch vanishes.

8. Acknowledgments

This work was supported by the U.S. Army Research Office, under a MURI grant DAAD19-00-1-0177.

References

1. K. K. Y. Wong, K. Shimizu, M. E. Marhic, K. Uesaka, G. Kalogerakis, and L. G. Kazovsky, "Continuous-wave fiber optical parametric wavelength converter with 40 dB conversion efficiency and a 3.8-dB noise figure," Opt. Lett. **28**, 692–694 (2003).
2. J. Hansryd, P. A. Andrekson, M. Westlund, J. Li, and P. Hedekvist, "Fiber-Based Optical Parametric Amplifiers and their Applications," IEEE J. of Sel. Top. in Quantum Electron. **8**, 506–520 (2002).
3. Y. Su, L. Wang, A. Agarwal, and P. Kumar, "Wavelength-Tunable All-Optical Clock Recovery Using a Fiber-Optic Parametric Oscillator," Opt. Comm. **184**, 151 (2000).
4. L. Wang, Y. Su, A. Agarwal, and P. Kumar, "Synchronously Mode-Locked Fiber Laser Based on Parametric Gain Modulation and Soliton Shaping," Opt. Commun. **194**, 313–317 (2001).
5. L. Wang, A. Agarwal, Y. Su, and P. Kumar, "All-Optical Picosecond-Pulse Packet Buffer Based on Four-Wave Mixing Loading and Intracavity Soliton Control," IEEE J. of Quantum Electron. **38**, 614–619 (2002).
6. J. L. Blows and S. E. French, "Low-noise-figure optical parametric amplifier with a continuous-wave frequency-modulated pump," Opt. Lett. **27**, 491–493 (2002).
7. R. Tang, J. Lasri, P. Devgan, J. E. Sharping, and P. Kumar, "Record performance of parametric amplifier constructed with highly nonlinear fibre," Electron. Lett. **39** (2003).
8. S. Radic, C. J. McKinstrie, R. M. Jopson, J. Centanni, Q. Lin, and G. Agrawal, "Record performance of parametric amplifier constructed with highly nonlinear fibre," Electron. Lett. **39** (2003).
9. P. L. Voss, R. Y. Tang, and P. Kumar, "Measurement of the photon statistics and the noise figure of a fiber-optic parametric amplifier," Opt. Lett. **28**, 549–551 (2003).
10. P. L. Voss and P. Kumar, "Raman-noise induced noise-figure limit for $\chi^{(3)}$ parametric amplifiers," Opt. Lett. **29**, 445–447 (2004).
11. P. Voss and P. Kumar, "Raman-effect induced noise limits on $\chi^{(3)}$ parametric amplifiers and wavelength converters," J. Optic. B. **6**, S762–S770 (2004).
12. R. Tang, P. L. Voss, J. Lasri, P. Devgan, and P. Kumar, "Noise-figure of a fiber parametric amplifier and wavelength converter: Experimental investigation," Opt. Lett. **29**, 2372–2374 (2004).
13. M. E. Marhic, C. H. Hsia, and J. M. Jeong, "Optical amplification in a nonlinear fiber interferometer," Electron. Lett. **27**, 201 (1991).
14. G. Bartolini, R. D. Li, P. Kumar, W. Riha, and K. V. Reddy, "1.5-mm phase-sensitive amplifier for ultrahigh-speed communications," in *Proc. OFC'94*, pp. 202–203 (1994).
15. C. M. Caves, "Quantum Limits on Noise in Limited Amplifiers," Phys. Rev. D **26**,

1817–1839 (1982).

16. W. Imajuku, A. Takada, and Y. Yamabayashi, "Inline coherent optical amplifier with noise figure lower than 3dB quantum limit," Electron. Lett. **36** (2000).
17. D. Levandovsky, M. Vasilyev, and P. Kumar, "Near-noiseless amplification of light by a phase-sensitive fibre amplifier," Pramana J. Phys. **2–3** (2001).
18. R. M. Shelby, M. D. Levenson, and P. W. Bayer, "Guided acoustic-wave Brillouin scattering," Phys. Rev. B **31**, 5244–5252.
19. K. Bergman, H. A. Haus, E. P. Ippen, and M. Shirasaki, "Squeezing in a Fiber Interferometer with a Gigahertz Pump," Opt. Lett. **19**, 290–292 (1994).
20. R. Tang, P. Devgan, P. L. Voss, V. Grigoryan, and P. Kumar, "An in-line frequency-nondegenerate phase-sensitive fiber-optical parametric amplifier," Submitted to Photon. Tech. Lett. (2004).
21. H. P. Yuen, "2-Photon Coherent States Of Radiation-Field," Phys. Rev. A **13**, 2226–2243 (1976).
22. H. P. Yuen and J. H. Shapiro, "Optical Communication With 2-Photon Coherent States .1. Quantum-State Propagation And Quantum-Noise Reduction," IEEE Trans. Inf. Theory **24**, 657–668 (1978).
23. J. H. Shapiro, H. P. Yuen, and J. A. M. Mata, "Optical Communication with 2-Photon Coherent States .2. Photoemissive Detection and Structured Receiver Performance," IEEE Trans. Inf. Theory **25**, 179–192 (1979).
24. H. P. Yuen and J. H. Shapiro, "Optical Communication with 2-Photon Coherent States .3. Quantum Measurements Realizable with Photo-Emissive Detectors," IEEE Trans. Inf. Theory **26**, 78–82 (1980).
25. C. M. Caves, "Quantum-mechanical noise in an interferometer," Phys. Rev. D **23**, 1693–1708 (1981).
26. J. H. Shapiro and L. Boivin, "Raman-Noise Limit on Squeezing in Continuous-Wave Four-Wave Mixing," Opt. Lett. **20**, 925–927 (1995).
27. L. Boivin, F. X. Kärtner, and H. A. Haus, "Analytical Solution to the Quantum Field Theory of Self-Phase Modulation with a Finite Response Time," Phys. Rev. Lett. **73**, 240–243 (1994).
28. F. X. Kärtner, D. J. Dougherty, H. A. Haus, and E. P. Ippen, "Raman noise and soliton squeezing," J. Opt. Soc. B **11**, 1267–1276 (1994).
29. N. R. Newbury, "Raman gain: pump-wavelength dependence in single-mode fiber," Opt. Lett. **27**, 1232–1234 (2002).
30. N. R. Newbury, "Pump-wavelength dependence of Raman gain in single-mode optical fibers," J. Lightwave Technol. **21**, 3364–3373 (2003).
31. D. J. Dougherty, F. X. Kärtner, H. A. Haus, and E. P. Ippen, "Measurement of the

Raman gain spectrum of optical fibers," Opt. Lett **20**, 31–33 (1995).

32. G. P. Agrawal, *Nonlinear Fiber Optics, Third Edition* (Academic Press, San Diego, CA, 2001).
33. F. Koch, S. A. E. Lewis, S. V. Chernikov, and J. R. Taylor, "Broadband Raman gain characterisation in various optical fibres," Electron. Lett. **37**, 1437–1438 (2001).
34. A. Boskovic, S. V. Chernikov, J. R. Taylor, L. Gruner-Nielsen, and O. A. Levring, "Direct continuous-wave measurement of n_2 in various types of telecommunication fiber at 1.55 mm," Opt. Lett. **21**, 1966–1968 (1996).
35. E. Golovchenko, P. V. Mamyshev, A. N. Pilipetskii, and E. M. Dianov, "Mutual influence of the parametric effects and stimulated Raman scattering in optical fibers," IEEE Journal of Quantum Electronics **26**, 1815–1820 (1990).